Available online at www.sciencedirect.com

SciVerse ScienceDirect

Polar Science 7 (2013) 188–203

http://ees.elsevier.com/polar/

Relationships between variations of the land–ocean–atmosphere system of northeastern Asia and northwestern North America

John E. Walsh [a,*], Hotaek Park [b], William L. Chapman [c], Tetsuo Ohata [b]

[a] *International Arctic Research Center, University of Alaska, Fairbanks, AK 99775-7340, USA*
[b] *Research Institute for Global Change, JAMSTEC, Yokosuka, Japan*
[c] *Department of Atmospheric Sciences, University of Illinois, Urbana, IL, USA*

Received 30 August 2012; revised 30 April 2013; accepted 1 May 2013
Available online 10 May 2013

Abstract

This study is a broad-scale synthesis of information on climate changes in two Arctic terrestrial regions, eastern Siberia and the Alaska–Yukon area of North America. Over the past 60 years (1951–2010), the trends of temperature and precipitation in the two regions are broadly similar in their seasonality. However, atmospheric advection influences the two regions differently during winter. The differential advective effects are much weaker in the other seasons. The Pacific Decadal Oscillation is the strongest correlator with interannual variability in the two regions, followed by the Arctic Oscillation and the El Niño/Southern Oscillation.

Projected changes by the late 21st Century are qualitatively similar to the changes that have been ongoing over the past 60 years, although the rate of change increases modestly under mid-range forcing scenarios (e.g., the A1B scenario). The greatest warming is projected to occur farther north over the Arctic Ocean in response to sea ice loss. Precipitation is projected to increase by all models, although increases in evapotranspiration preclude conclusions about trends toward wetter or drier land surface conditions. A notable feature of the future climate simulations is a strong maximum of pressure decreases in the Bering Sea region, implying further advective changes.

Keywords: Climate; Arctic; Siberia; Alaska

1. Introduction

It is well known that recent climate change has been greater in higher latitudes than in middle latitudes of the Northern Hemisphere (ACIA, 2005; AMAP, 2011). This so-called "polar amplification" is due to a combination of factors, including the albedo-temperature feedback, increased atmospheric water vapor, and increased transports of heat and moisture into the Arctic (e.g., Bekryaev et al., 2010). The conclusion of the IPCC (2007) is that at least some of the recent warming, as manifested in the polar-amplified warming of the past century, is attributable to external forcing associated with human activities. However, the high latitudes of the Northern Hemisphere are spatially heterogeneous, containing features ranging from continental landmasses to the Greenland ice sheet to relatively warm northward-flowing ocean currents. Thus the variations and changes of climate over decadal-to-centennial timescales cannot be expected to be uniform over a pan-Arctic domain. Moreover, the

* Corresponding author. Tel.: +1 907 4 74 2677.
E-mail address: jwalsh@iarc.uaf.edu (J.E. Walsh).

1873-9652/$ - see front matter © 2013 Elsevier B.V. and NIPR. All rights reserved.
http://dx.doi.org/10.1016/j.polar.2013.05.002

driving by the large-scale atmosphere, with its mid-latitude interactions and its variations over a spectrum of timescales, further complicates the detection and diagnosis of climate change in high latitudes.

In the present paper, we provide a diagnostic evaluation of climate changes over the past 60 years in two adjacent subregions of the Arctic: the eastern Siberian region of Asia and the Alaska–Yukon region of North America. These two regions are separated by the narrow Bering Strait, and are the foci of a variety of field projects and modeling studies in the JAMSTEC-IARC Collaboration Study (Hinzman, 2013). The present paper is intended to provide a background depiction of ongoing change in the two regions, thereby setting the stage for various other more targeted studies reported in this special issue.

Both the eastern Siberian and Alaska/Yukon regions are characterized by relatively cold climates with large seasonal amplitudes (at least away from the immediate coastal zones. Both regions contain large river basins (Fig. 1) and extensive areas of permafrost. Yet the drivers of climate changes in these two regions can be quite different, and the responses to climate drivers in these two regions can also be quite different (e.g., Park et al., 2013). In the present paper, we examine recent changes in these regions by documenting (1) the consistency of climate changes on the two sides of Bering Strait over the past 60 years, (2) the seasonality of the trends, (3) drivers of the recent variations, and (4) projections of future changes of climate in the two regions. While the emphasis is on the primary climate variables (temperature, precipitation, atmospheric circulation), we supplement the analysis with some information on soil moisture and snow depth in the largest river basins (the Lena and the Mackenzie) of each region (Fig. 1).

Fig. 1. Major river basins of northwestern North America and northeastern Asia. Source: National Oceanic and Atmospheric Administration, http://www.arctic.noaa.gov/detect/land-river.shtml

2. Data and methods

One of the primary tools used in for diagnostic analysis is the NCEP/NCAR reanalysis (Kistler et al., 2001). While other reanalyses exist (e.g., ERA-40 and ERA-Interim, JRA, NASA MERRA, the North American Regional Reanalysis), the NCEP/NCAR reanalysis has the longest time span, as it begins in 1948 and is updated through the present. Since priorities in this study are maximum record length and coverage beyond North America, the NCEP/NCAR reanalysis is the logical choice for the primary input.

The NCAR/NCEP reanalysis uses a global spectral model and a spectral statistical interpolation analysis scheme to assimilate observational data and provide gridded output in four classes of variables. Class A is an analysis variable strongly influenced by observations. Of the variables examined in this study, sea level pressure is a class A variable. Class B variables have both an observational and model contributions to the output variables. Air temperature is a class A variable above the surface but a class B variable at the surface. Class C indicates a variable solely derived from the model, and class D represents a field obtained from climatological values with no influence from the model. Notable variables in class C are precipitation, potential and actual evapotranspiration, soil moisture and runoff. Output from the reanalysis spans the period from 1948 to present and has a global spatial resolution of 2.5°. The variables are 6 hourly averages, archived as daily averages, monthly averages, and other long-term means.

A potential risk in the use of reanalyses arises from changes in the input streams of assimilated data. In the case of the Arctic, for example, the ingestion of satellite data for upper air variables (e.g., temperature) began in the 1970s, while the sea level pressure observations of the International Arctic Buoy Network became available in 1979. Gleicher et al. (2011) examined the Arctic sea level pressure fields for discontinuities in 1979, and found that differences of the 30-year means before and after 1979 were smaller than the natural variability of 30-year means. Serreze et al. (2003a,b) and others have found precipitation fields the NCEP/NCAR reanalysis to be problematic. However,

Serreze et al. did use these fields as an aid in reconstructing precipitation fields for the northern terrestrial watersheds over a 30-year period centered on the 1970s, while Zhang et al. (2004) and Mesquita et al. (2010) used the same reanalysis to produce time series of high-latitude storminess from 1948 through the early 2000s. None of these studies showed discontinuities in the late 1970s. Bromwich et al. (2007) describe a more comprehensive assessment of atmospheric reanalyses in the polar regions, concluding that there are indeed major problems in the Antarctic with discontinuities in the late 1970s but that the problems are much less severe in the Arctic. In view of the absence of demonstrated heterogeneities in the Arctic in these various studies, we use the NCEP/NCAR reanalysis for our full study period, 1951–2010, although for surface air temperature and precipitation we utilize independently compiled gridded analyses of station measurements.

Several supplementary datasets of temperature and precipitation were also utilized. The first is the University of Delaware's gridded database of surface air temperature and precipitation based on station measurements. The second is the gridded database of surface air temperatures from the University of East Anglia, U.K. Since the values in these datasets are based entirely on *in situ* measurements by surface stations, they are free from the model influences that can impact reanalysis-derived fields. However, such station-based datasets are limited to land only, as marine/ship reports are not included. The University of Delaware datasets are available from the Earth System Research Laboratory of the National Oceanic and Atmospheric Administration (http://www.esrl.noaa.gov/psd/data/gridded/data.UDel_AirT_Precip.html). The University of East Anglia temperature dataset is available at http://www.cru.uea.ac.uk/cru/data/temperature

In Section 3, we present fields of several derived variables obtained from other sources. "Annual thaw index" is an accumulation of daily temperature exceedances of 0 °C (thawing degree days) during the warm season, based on Hirabayashi et al.'s (2008) gridded surface air temperatures (used to force the CHANGE land surface model (Park et al., 2013). Soil moisture, simulated by the land surface model (not the NCEP/NCAR reanalysis), represents the averaged soil water for the period of June to August, less the ice amount, in the upper 1.6 m. The winter-averaged simulated snow depth is also obtained from the land surface model.

Finally, time series of several indices of major modes of ocean–atmosphere variability are used. These modes include the Pacific Decadal Oscillation (PDO), the Southern Oscillation Index (SOI) and Niño 3–4 sea surface temperature anomalies associated with the El Niño phenomenon in the tropics, and the Arctic Oscillation (AO). These indices are compiled by the Climate Prediction Center of the National Centers for Environmental Prediction and are available through the Earth System Research Laboratory at http://www.esrl.noaa.gov/psd/data/climateindices/

The methods for assessing recent changes and associations with atmosphere/ocean drivers are kept relatively simple insofar as this study is an attempt to compare and attribute variations in two adjacent subregions of the Arctic. These subregions are (1) northeastern Asia, defined as 50°–80°N, 120°–180°E, and (2) northwestern North America, defined as 50°–80°N, 180°–120°W; when a particular data source is available for land areas only (e.g., the University of Delaware and the East Anglia datasets noted above), the analysis is made for only the land areas within the two latitude–longitude sectors. Changes over the 60-year period, 1951–2010, are examined in terms of fields of composite differences between the means for two 30-year subperiods: 1981–2010 minus 1951–1980. The differences therefore correspond to the changes from the earlier 30-year period to the most recent 30-year period. Because they are based only on two sets of 30-year means at each grid point, they do not capture the variations within each subperiod. The advantage of the composite difference approach is that the differences are less sensitive than linear regression-derived trends to large anomalies at the beginning or end of the time series. We do, however, illustrate the corresponding within-period interannual variations of surface air temperatures for each season in each region. Shorter-term variability is incorporated into the analysis by the use of linear correlations between the main climate variables (e.g., temperature, precipitation) and the indices of the major modes of atmosphere–ocean variability. The correlations are computed directly from the unsmoothed, non-detrended data. While indices of two of the major modes of variability (Pacific Decadal Oscillation and El Niño/Southern Oscillation) show year-to-year autocorrelation, the seasonal and annual values of the atmospheric variables show essentially no year-to-year autocorrelation. The correlations are evaluated for the entire 60-year period and displayed as maps of the correlations at the grid points in the two regions and the surrounding area.

In the following section, we illustrate changes in annual and seasonal means between the two 30-year periods spanned by 1951–2010. The conventional definitions are used for the seasons: winter

(December–February), spring (March–May), summer (June–August), autumn (September–November). In order to have 30 full winters in the first 30-year period, the first winter includes December 1950.

3. Results

3.1. Recent changes within the 1951–2010 time period

Fig. 2 shows time series of the annual temperatures averaged over the two regions, Siberia and Alaska–Yukon. The plotted values for each region are departures from the respective 60-year means. While there is a weak correlation between interannual variations in the two regions, the outstanding feature of Fig. 2 is the general increase of temperature through the 60-year period. The means for 1981–2010 are about 1 °C warmer than the means for 1951–1980, as will be apparent in the spatial maps presented below. Fig. 3 shows the corresponding seasonal time series, highlighting the much greater interannual variability in winter than in summer. The underlying trends are positive in both regions in all seasons, although the autumn trend for Alaska–Yukon is close to zero and positive only because of the relative warmth of several years in the final decade. Notably, the correlations of the detrended interannual variations are generally insignificant, pointing to a role of atmospheric circulation anomalies for which the advective temperature impacts differ in the two regions. We provide specific examples of these impacts in Section 3.2.

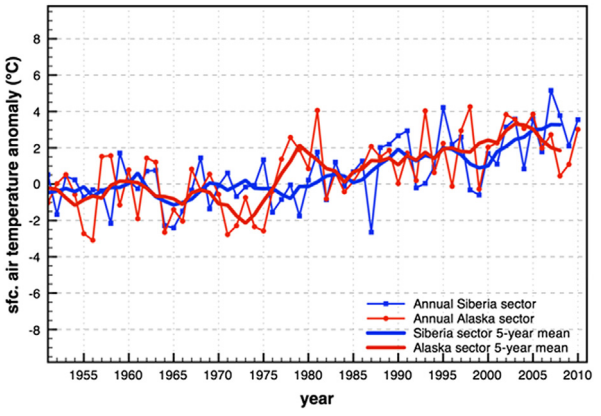

Fig. 2. Time series of annual temperatures for 1951–2010, plotted as departures from 60-year means, for Alaska/Yukon (red) and eastern Siberia (blue). Thin lines show yearly values, thick lines are 5-year running means. (For interpretation of the references to colour in this figure legend, the reader is referred to the web version of this article.)

The signature of polar amplification is apparent in the change of annual mean temperatures from 1951–1980 to 1981–2010 (Fig. 4). Maximum warming of more than 2 °C has occurred offshore of the Siberian coast, where sea ice has shown a large retreat during the warm season (Stroeve et al., 2011). The change in annual mean temperature over much of terrestrial region of eastern Siberia and the Alaska/Yukon region is about 1 °C. However, the annual mean pattern obscures a strong seasonality in the temperature change. As shown in Fig. 5a, the winter warming is much greater over Alaska and the Yukon than in eastern Siberia, where the trend is small and even negative (cooling) in some areas. The main area of cooling is over the extreme northwestern Pacific Ocean east of Kamchatka, although there is also an area of cooling in the Sea of Okhotsk. The western North Pacific is one of the few areas of the Northern Hemisphere to have cooled during winter over the past 50–60 years. The winter warming over much of Alaska is about 2 °C, and it is even larger in the Yukon and western Canadian Archipelago region. The springtime pattern (Fig. 5b) is qualitatively similar to the winter pattern, although the magnitudes of the changes are muted, especially over the Alaska–Yukon region. Weak warming (<1 °C) characterizes the summer changes nearly everywhere in the domain, over both land and ocean, except for an area of weak cooling over southeastern Alaska and the southwestern Yukon. By contrast, the autumn pattern shows strong warming (>2 °C) over most of the Arctic Ocean, including the seas north of the Alaskan and Siberian coasts, while most of the Alaska–Yukon region has cooled slightly. The autumn warming maximum over the Arctic Ocean is consistent with the seasonality of the sea ice reduction, which has been largest in late summer and autumn.

As noted earlier, precipitation is a class C (model-derived) variable in reanalyses. Reanalysis-derived precipitation amounts are known to be problematic, and the NCEP/NCAR reanalysis is no exception (Serreze et al., 2005). For this reason, we base our evaluation of 60-year changes on the University of Delaware precipitation dataset, which is based entirely on station data. Fig. 6 shows the distribution of changes in seasonal mean precipitation from 1951–1980 to 1981–2010. Summation over all seasons and the entire terrestrial domain in Fig. 6 shows that the positive changes slightly outweigh the negative in all seasons except winter. The area-averaged changes of the 30-year means from the 1951–1980 to 1981–2000, expressed as percentages of the means

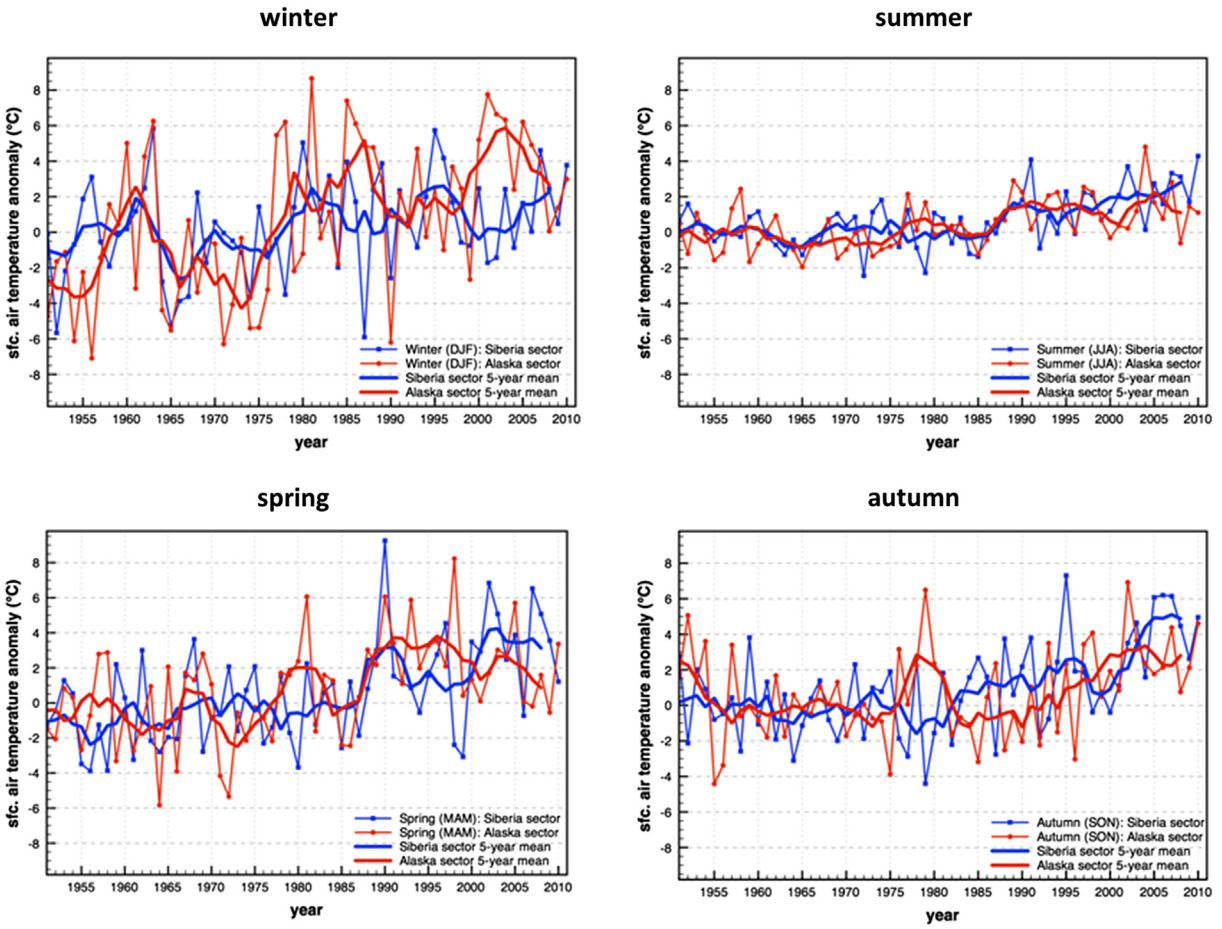

Fig. 3. Time series of departures from mean seasonal temperatures for winter (Dec–Feb), spring (Mar–May), summer (Jun–Aug) and autumn (Sep–Nov). Red lines are for Alaska/Yukon, blue lines are for eastern Siberia. Thin lines show yearly values, thick lines are 5-year running means. (For interpretation of the references to colour in this figure legend, the reader is referred to the web version of this article.)

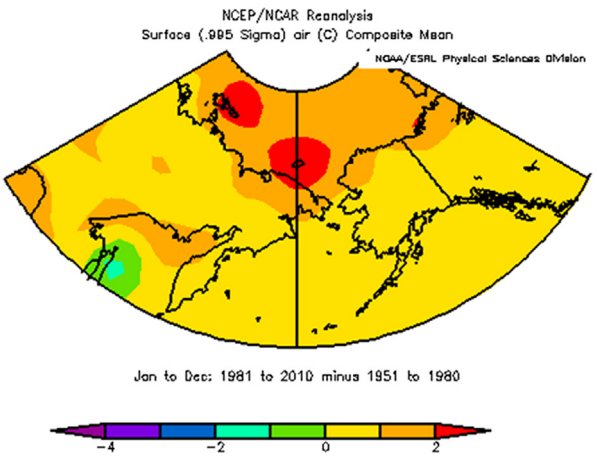

Fig. 4. Changes of 30-year annual mean temperature (°C) from 1951–1980 to 1981–2010.

for 1951–1980, are approximately −5% for winter, +1% for spring, +4% for summer and +8% for autumn. The seasonally integrated changes, weighted by the fractions (largest in summer and autumn) of the annual precipitation occurring in each season, are consistent with the Arctic-wide increase of annual precipitation by about 5% since 1950 (Walsh et al., 2011). Notable features in Fig. 6 include the decreases during winter in the southeastern Siberia and the West Coast of Canada; smaller decreases in these same areas during spring together with increases in far eastern Russia; summer decreases over western Alaska, particularly the southwestern part of the state, together with increases in western Canada and the region north of the Sea of Okhotsk; and a predominance of increases in autumn, except for Alaska.

Sea level pressure is a measure of the atmosphere circulation that is responsible for variations of near-

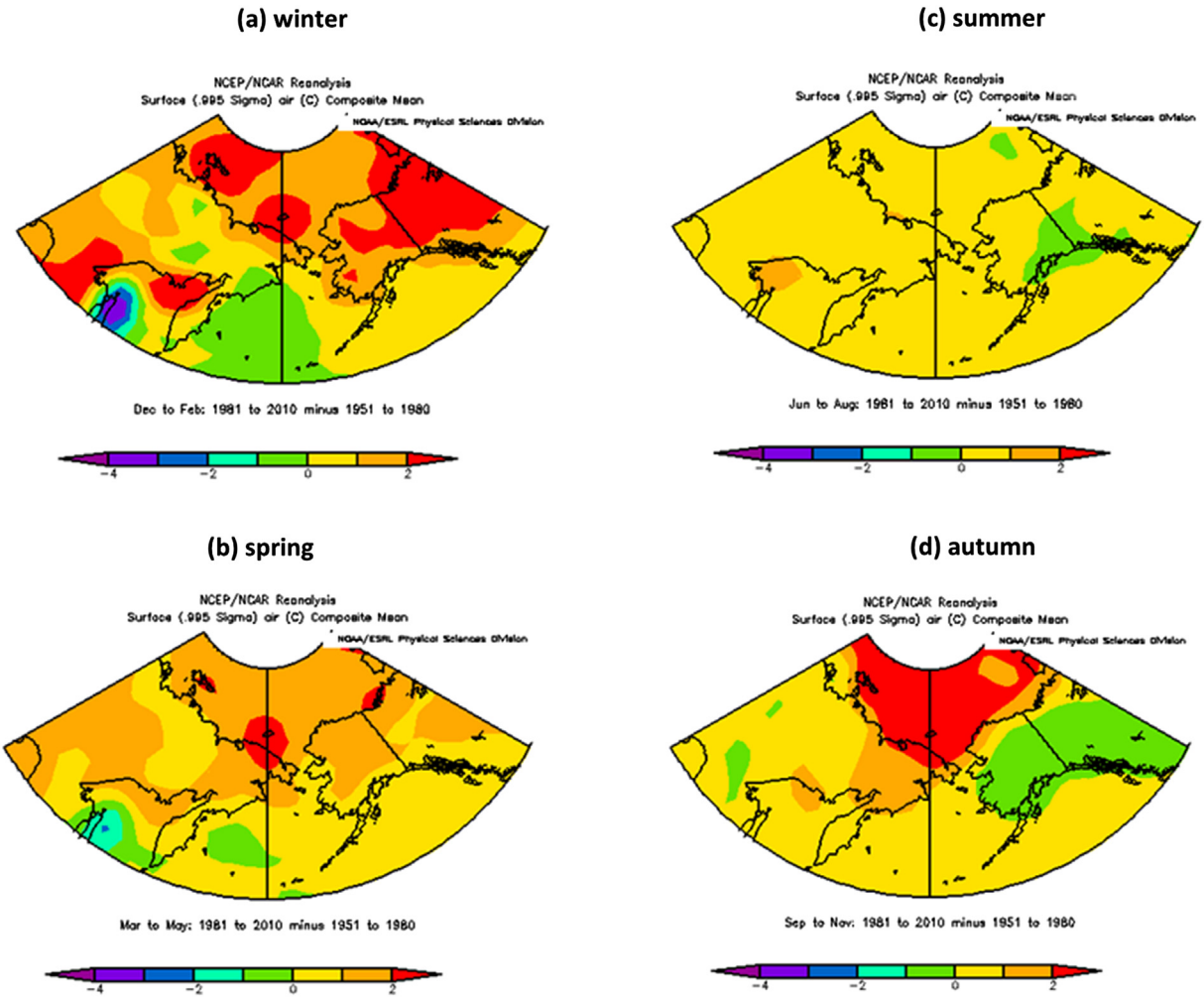

Fig. 5. Changes of 30-year seasonal mean temperature (°C) from 1951–1980 to 1981–2010: (a) winter, (b) spring, (c) summer, (d) autumn.

surface temperature and precipitation over timescales of days to years and even decades. Indeed, one of the great challenges in the attribution of climate change is distinguishing the effects of external forcing from internal variability manifested in the atmospheric circulation. The attribution challenge is further complicated by the possibility that the modes of atmosphere–ocean circulation can also change in response to external forcing. Fig. 7a shows the changes in the mean winter sea level pressure fields from the 1951–1980 period to the subsequent 1981–2010 period. Pressures decreased over nearly the entire domain, with the largest decreases (3–4 hPa) over the region of the Aleutian low and the area northwest of the Sea of Okhotsk. The gradient wind changes corresponding to Fig. 7a correspond to increased southerly airflow (warm advection) over the Alaska–Yukon region and increased northerly airflow over far eastern tip of Siberia, opposing incursions of mild Pacific air into far eastern Siberia. These changes are broadly consistent with the wintertime temperature changes in Fig. 5a, which show a maximum warming over Alaska–Yukon and an area of cooling west of the Aleutians and extending into the eastern-most portion of Siberia. However, the pattern in Fig. 7a is too broad-brush to capture the impacts of any shifts that occur more than a few years from 1980, and the pattern does not depict circulation changes that occurred over time scales shorter than the seasonal average.

Fig. 7b shows the changes of summertime sea level pressure between the two 30-year subperiods. The changes are small and inconsequential for advective temperature changes, as are the changes in spring and autumn (not shown). We conclude that the atmospheric

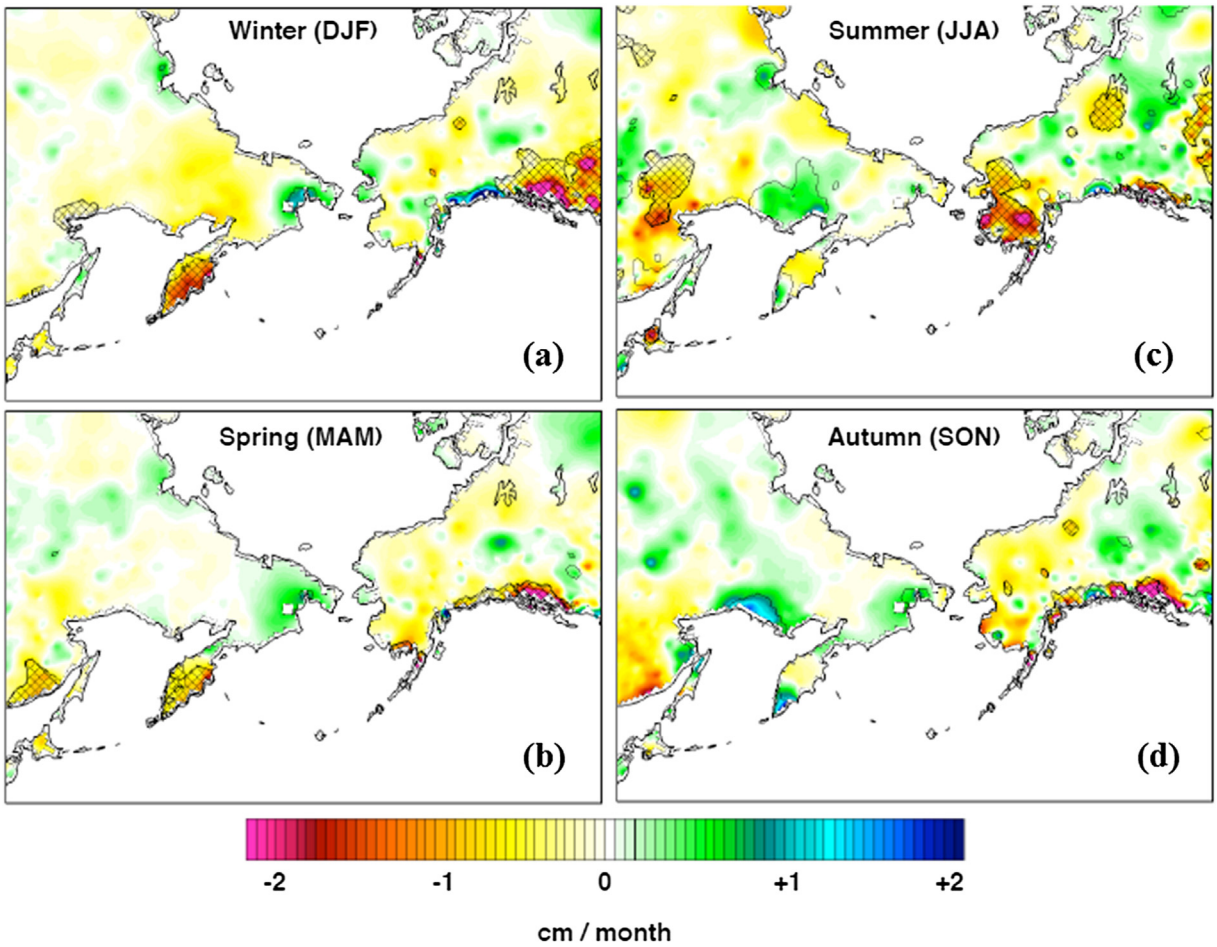

Fig. 6. Changes of 30-year seasonal mean precipitation (cm month^{-1}) from 1951–1980 to 1981–2010 for (a) winter, (b) spring, (c) summer, (d) autumn.

circulation can explain little or no portion of the pre-to-post-1980 changes in average temperature for those seasons. External (radiative) forcing, more localized natural variability, and surface changes and feedbacks are candidate explanations for the observed changes in temperature and precipitation during spring, summer and autumn.

The preceding discussion has addressed three primary atmospheric variables (temperature, precipitation, sea level pressure) that characterize the near-surface atmosphere. Responses to trends and variations in these atmospheric variables occur in the terrestrial system, which in high latitudes includes permafrost and snow cover and their interactions with soil moisture. A recent study (Park et al., 2013) has addressed variations in these quantities in the major river basins of the Arctic drainage area. As illustrative examples, we present in Fig. 8 several time series of anomalies of surface quantities averaged over the Lena and the Mackenzie River Basins, which occupy the western and eastern portions of the domain addressed in this study. The plotted variables are the annual thawing index (ATI), which is the accumulation of thawing-degree days over the warm season; soil moisture (SM); and winter-averaged snow depth (SD).

Soil moisture and snow depth are potentially problematic quantities in a reanalysis, as they are not assimilated directly. Snow cover is prescribed based on weekly historical analyses of snow cover (Kalnay et al., 1996). Soil moisture in the NCEP/NCAR reanalysis is nudged toward an assumed climatology, which is known to introduce bases into soil moisture and evapotranspiration in middle latitudes (Maurer et al., 2001). As a result, the NCEP/NCAR soil moisture show less anomaly persistence than observations and later reanalyses (Lu et al., 2005), Lu et al. (2005) also

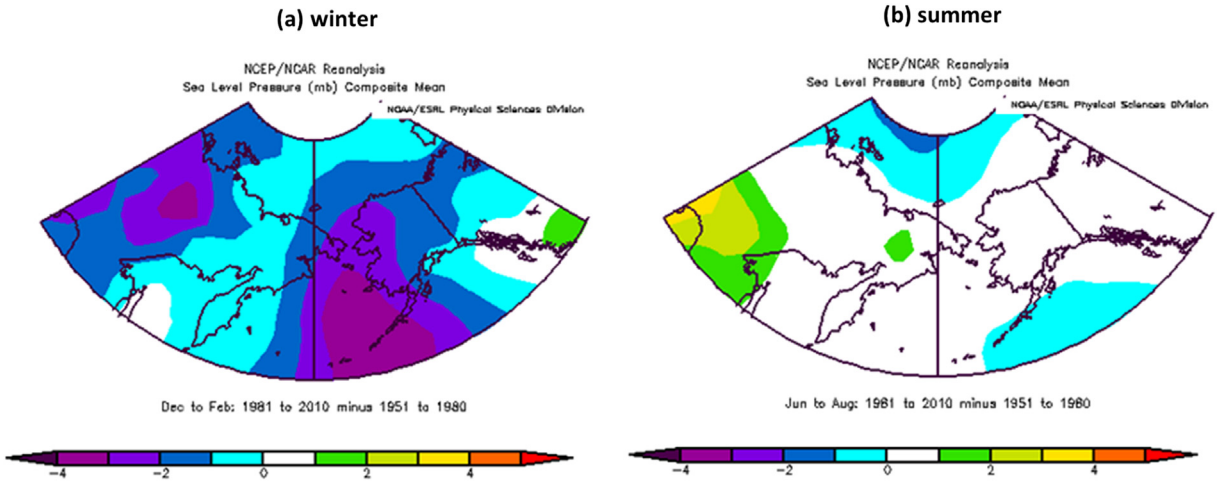

Fig. 7. Changes of 30-year seasonal mean sea level pressure (hPa) from 1951–1980 to 1981–2010 for (a) winter and (b) summer.

found that the seasonal cycle of soil moisture was greater in the reanalysis than in observational data. However, the database for validation is very sparse in our subregions, which are characterized by substantial areas of permafrost. The land surface module used in the reanalysis does not include the latent heat of fusion in the seasonal phase changes of the permafrost active layer. For these reasons, we did not use the soil moisture and snow depth from the NCEP/NCEP reanalysis; we instead show results for these variables from the CHANGE land surface model (Park et al., 2013) simulations of the same time period for which our other variables are analyzed.

It is apparent from Fig. 8a that the annual thawing index has increased since 1960 in both river basis, consistent with the changes of temperature in summer, spring and autumn (Fig. 5). While soil moisture computed from a land surface model (Park et al., 2013) shows little systematic change in either river basin, there has been a substantial decrease in winter-averaged snow depth in the Mackenzie Basin. This decrease is consistent with the warming in spring (Fig. 5b), together with the decrease of precipitation over much of the Mackenzie Basin during winter (Fig. 6a). In the Lena Basin, on the other hand, there have been slight increases of precipitation in autumn, winter and spring, favoring a snowfall increase. This increase of snowfall tends to counteract the shortening of the snow season caused by warming temperatures. Specifically, more snowfall during winter requires additional time to melt in the spring, even if snow does not fall as late into the spring season as in the previous decades. Greater winter snowfall also favors an increase of springtime runoff, and such an increase has been reported by Zhang et al. (2013), who have recently shown that the increase of Siberian river discharge is consistent with increased atmospheric water vapor convergence, which is greatest during the winter season. Zhang et al.'s study included the record discharge year of 2007 and the high-discharge year of 2008, which were not included in Shiklomanov et al.'s (2007) earlier study that showed a decrease of cold-season precipitation in the Lena Basin.

3.2. Role of teleconnections in short-term climate variations

While the preceding discussion has emphasized changes of the means of atmospheric variables between successive 30-year periods, there are also substantial interannual and multiyear variability within each subperiod (e.g., Figs. 2 and 3). This variability, upon which longer-term trends are superimposed, is driven largely by the atmospheric circulation and corresponding ocean anomalies. In this section we examine spatial patterns associated with the major modes of variability in the atmosphere–ocean system. These modes include the El Niño/Southern Oscillation phenomenon, which is tracked by various metrics, including (1) the Southern Oscillation Index and (2) ocean temperature anomalies in the so-called Niño 3.4 region of the eastern equatorial Pacific Ocean; (3) the Pacific Decadal Oscillation (PDO); and (4) the Arctic Oscillation (AO). While other modes of atmosphere–ocean variability have been documented and are routinely monitored, the four modes listed above have spatial signatures that make them candidates for impacts on the northern terrestrial regions on which this

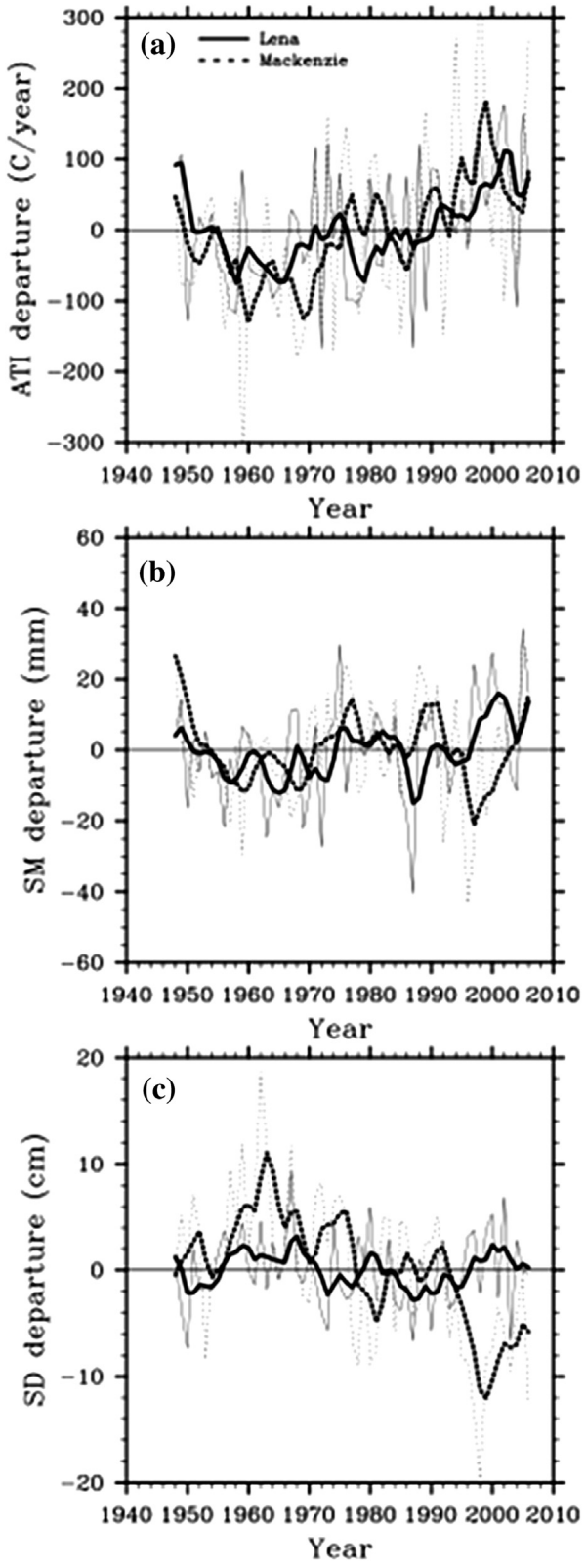

Fig. 8. Time series of (a) Annual thaw index, ATI (see text), (b) soil moisture, SM; and (c) snow depth (SD) in the Lena River Basin (solid lines) and the Mackenzie River Basin (dashed lines). Gray lines are annual departures from period-of-record means, black lines are low-pass filtered values. From Park et al. (2013).

study focuses. Time series of the four indices are shown in Figs. 9 and 10. We note here that the Southern Oscillation Index and the Niño 3.4 ocean temperatures are both indices of ENSO, the El Niño/Southern Oscillation. The Southern Oscillation Index, which is the normalized difference in sea level pressure anomalies between Tahiti and Darwin, is an atmospheric index with greater high-frequency variability than the more persistent Niño 3–4 ocean temperature anomalies. We examine correlations with both ENSO indices in order to determine whether their different timescales of variability affect the strength of their associations with variations over the northern land areas.

In order to illustrate the role of these atmosphere–ocean modes in the variability over the Pacific subarctic, we have constructed spatial correlation maps for each season, for each of the four atmosphere–ocean modes listed above, and for each of the atmospheric variables addressed in Section 3.1 (air temperature, precipitation, sea level pressure). Because many of the spatial correlation maps did not contain strong or significant features over the Siberian and/or Alaska/Yukon regions, we limit the presentation to several illustrative examples of correlation maps that do represent significant associations.

Fig. 11 shows the correlation between the wintertime Pacific Decadal Oscillation (PDO) index and the temperature at 850 hPa over an expanded North Pacific domain. Positive correlations exceeding 0.7 are found over the Alaska–Yukon region, while negative values of −0.6 and lower are found in the North Pacific southwest of the Aleutians. These correlations are highly significant statistically, as the 95% and 99% significance levels are approximately 0.31 and 0.41, respectively, after the sample sizes are reduced on the basis of the autocorrelations (Ebisuzaki, 1997). The strong correlation with Alaskan temperatures has been noted by Hartmann and Wendler (2005). This pattern is very consistent with the change in the means between the two recent 30-year subperiods (Fig. 5a), pointing to the importance of the PDO as a driver of multidecadal variability (and hence trends) in this region. It provides an example of the role of advective forcing in low-frequency variations of air temperature. The pattern in Fig. 11 also appears in other season although, especially in summer, it is considerably muted relative

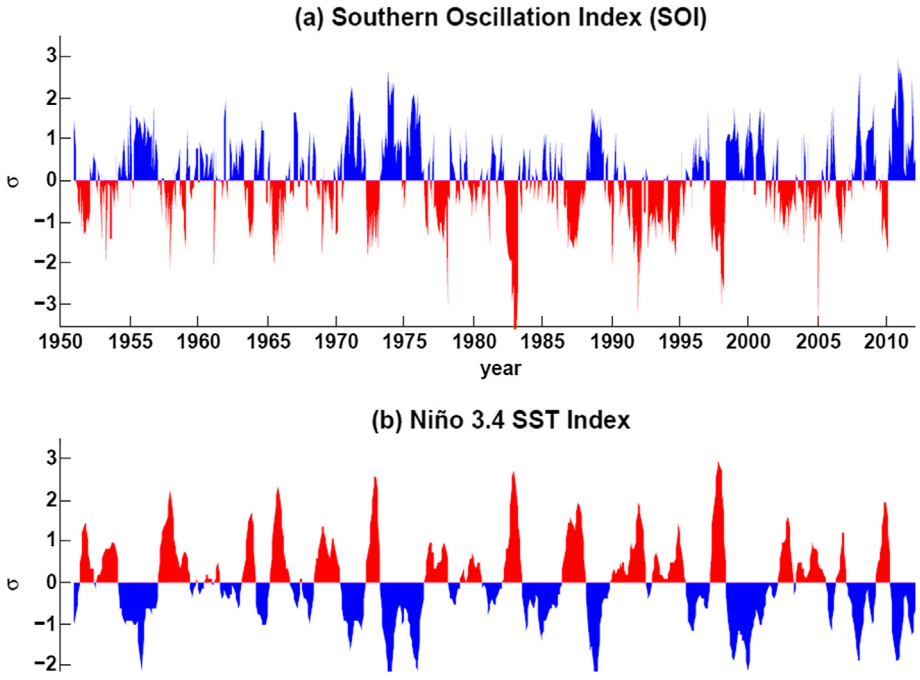

Fig. 9. Time series of (a) Southern Oscillation Index and (b) Niño 3.4 sea surface temperature index. Red denotes conditions corresponding to El Niño events (positive Niño 3.4 SST anomalies, negative SOI); blue denotes conditions corresponding to La Niña events (negative SST anomalies, positive SOI). All units are standard deviations, σ, of departures from means for the period. (For interpretation of the references to colour in this figure legend, the reader is referred to the web version of this article.) Data source: NOAA Pacific Marine Environmental Laboratory, http://www.pmel.noaa.gov/pubs/outstand/mcph2969/mcph2969.shtml

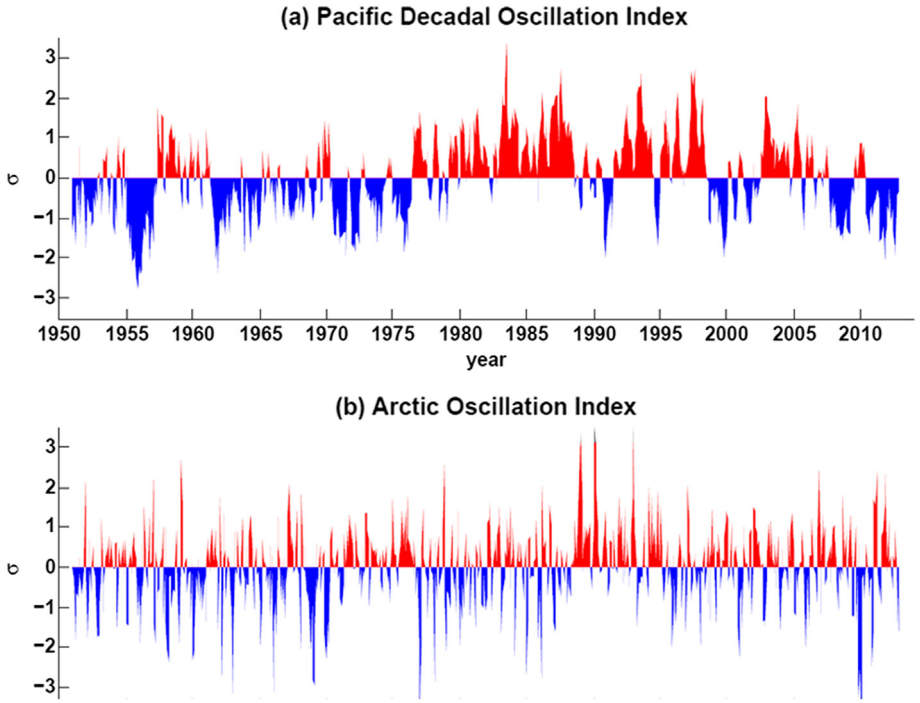

Fig. 10. Time series of indices of (a) Pacific Decadal Oscillation and (b) Arctic Oscillation. All units are standard deviations, σ, of departures from means for the period. Data sources: (a) University of Washington (http://jisao.washington.edu/pdo/graphics.html) and (b) National Center for Atmospheric Research (https://climatedataguide.ucar.edu/sites/default/files/cas_data_files/asphilli/nam_pc_djfm.txt).

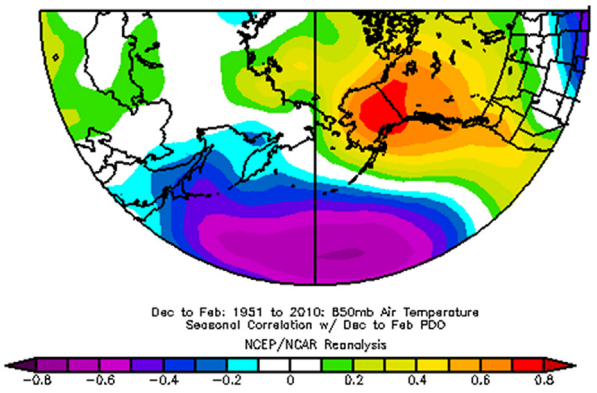

Fig. 11. Correlations between winter (Dec–Feb) air temperatures at 850 hPa and the winter Pacific Decadal Oscillation (PDO) index for the period 1951–2010.

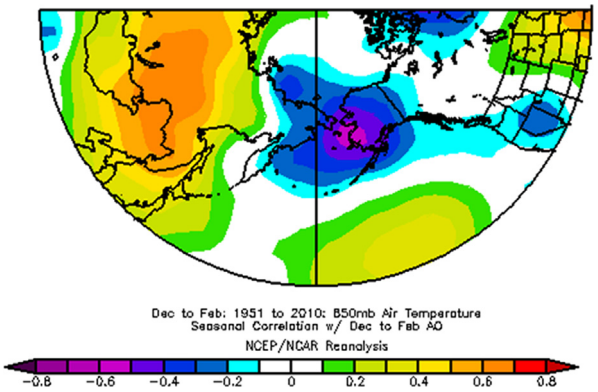

Fig. 12. Correlations between winter (Dec–Feb) air temperatures at 850 hPa and the winter Arctic Oscillation (AO) index for the period 1951–2010.

to Fig. 11. While the PDO evidently plays an important role in northwestern North America's winter temperature variability, it does not play a role over the eastern Siberian region containing the Lena Basin and the Kolyma Basin (except for a small area near the outlet of the Kolyma River).

Fig. 12 shows the wintertime correlations between the Arctic Oscillation (AO) and the 850 mb temperatures. This signal is also quite strong, as the magnitudes exceed 0.6 over western Alaska (negative values) and over Siberia (positive values). As in Fig. 11, the 95% and 99% thresholds of statistical significance are approximately 0.31 and 0.41. The role of the AO as a contributor to decadal-scale variations of temperature over Asia has been noted by Wallace and Thompson and Wallace (2000), but Fig. 12 indicates that the Alaskan association is also quite large over the 60-year period 1951–2010. Relative to the PDO correlation pattern in Fig. 11, the inflection point between the two lobes of correlation is shifted westward into eastern Siberia, so the PDO- and AO-driven temperature anomalies will generally not optimally reinforce (or oppose) each other when their amplitudes are both large. The signature of the AO is also weaker in middle latitudes than in higher latitudes, in contrast to the PDO correlation pattern in Fig. 11.

An east–west dipole of correlations with terrestrial surface air temperatures is driven by the El Niño/Southern Oscillation phenomenon. Fig. 13 shows the correlations of winter surface air temperatures over land with (a) the December–February Southern Oscillation Index and (b) the sea surface temperature anomalies in the Niño 3–4 region of the eastern tropical Pacific. Because the SOI is negative when ocean temperature anomalies are positive in the eastern

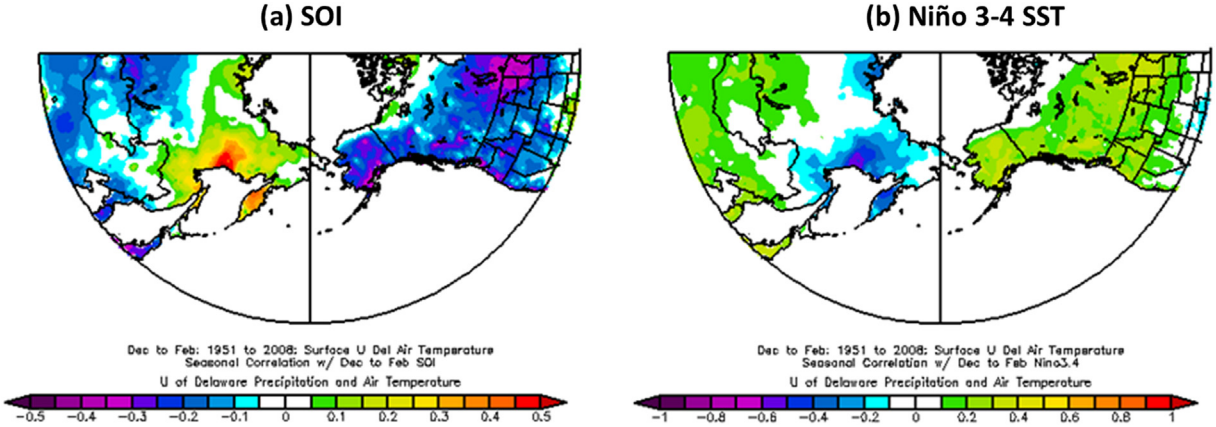

Fig. 13. Correlations between winter (Dec–Feb) surface air temperature and (a) the winter Southern Oscillation Index, (b) Niño 3–4 winter sea surface temperatures.

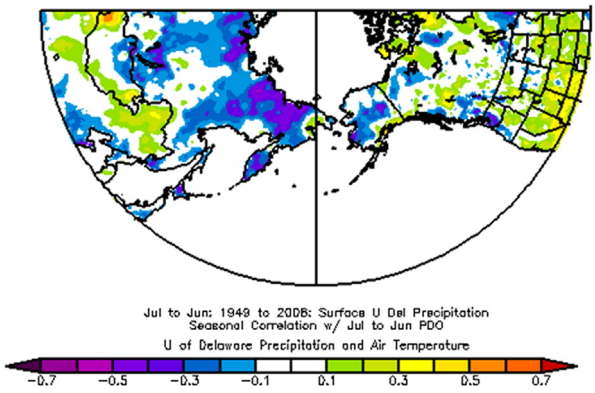

Fig. 14. Correlations between 12-month (July–June) precipitation and corresponding values of the Pacific Decadal Oscillation (PDO) index.

tropical Pacific, the correlation patterns are opposite in sign. The two correlation patterns are similar, indicative of the highly negative correlation between the two indices, with magnitudes are as large as ±0.4 over Alaska and far eastern Siberia. With regard to the mechanism underlying the correlation pattern, an El Niño event (negative SOI, positive Niño 3–4 ocean temperature anomalies) leads to an intensification of the Aleutian low, enhancing the inflow of warm maritime air into northwestern North America and enhancing northerly airflow into far eastern Siberia; the Aleutian low weakens during a La Niña event. The maximum correlations with the Niño 3–4 index are slightly larger than those with the SOI (note the different scales of the two color bars in Fig. 13), suggesting some dilution of the correlations by the high-frequency noise in the SOI. However, the correlations with both the SOI and the Niño 3–4 indices over the two northern areas are generally weaker than those with the PDO, consistent with the PDO's stronger manifestation in ocean temperatures and atmospheric pressures in middle latitudes vis-a-vis the ENSO's stronger manifestation in the tropics. The ENSO correlation patterns are also weaker than those of the AO in the high-latitude areas considered here. The ENSO correlations are even weaker in other seasons than in winter.

Finally, the associations between northern terrestrial anomalies and atmosphere/ocean modes are not limited to air temperature. Fig. 14 shows that yearly

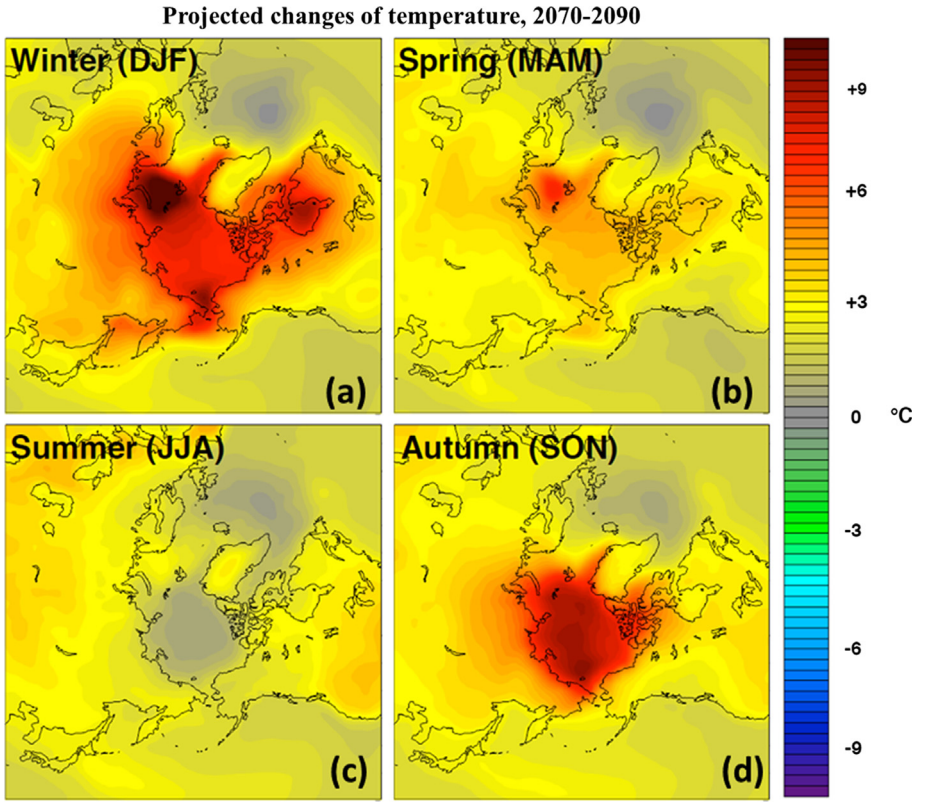

Fig. 15. Projected changes of temperature by season for 2070–2090. Projections are shown for (a) winter, (b) spring, (c) summer and (d) autumn. Changes are composited over the CMIP3 models forced by the A1B scenario.

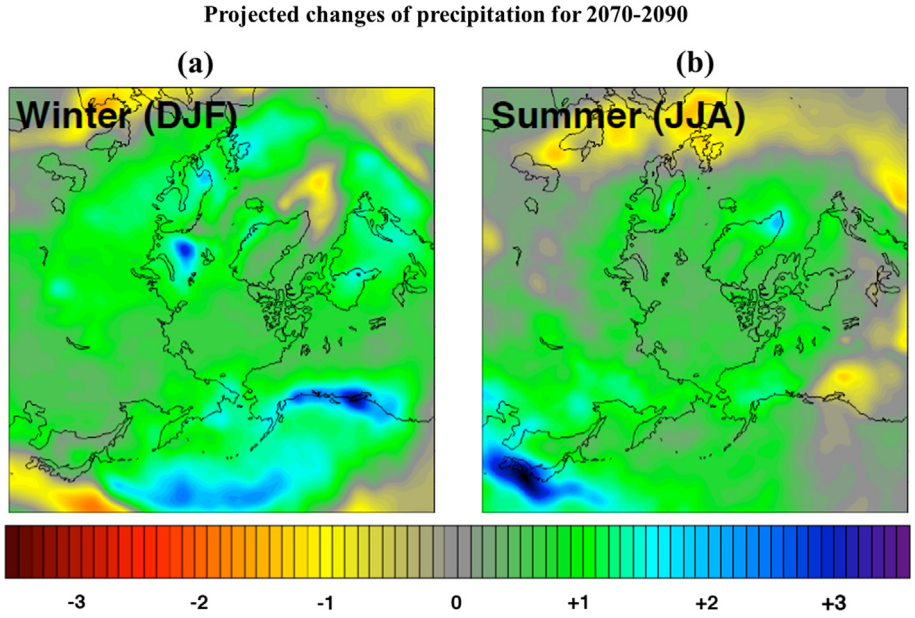

Fig. 16. Projected changes of (a) winter and (b) summer precipitation for 2070–2090 based on composite of CMIP3 simulations forced by the A1B scenario. Units are cm.

precipitation over interior Alaska and especially over eastern Siberia is negatively correlated with the PDO. (In this case, the correlations are for the 12-month period, July through June, centered on the winter season, as the PDO signal is strongest in winter). The implication of Fig. 14 is that, when the PDO is in its positive phase (warm SST anomalies in the eastern North Pacific, cool anomalies in the western North Pacific), drier-then-normal conditions are likely over interior Alaska and eastern Siberia. Given the low-frequency component of the PDO, this association introduces modest predictive potential with respect to precipitation anomalies in the northern terrestrial regions.

3.3. Future projections

With the preceding sections providing the background of ongoing changes and drivers of variability, we present here a brief summary of the changes projected for the Alaska/Yukon and Siberian regions by the late 21st Century. These projections are composites of the A1B simulations by 15 CMIP3 (Coupled Model Intercomparison Project) models used in the IPCC's Fourth Assessment Report (IPCC, 2007). The selection of the models and the compositing procedure are described by Chapman and Walsh (2007). The projected changes shown in this section (Figs. 15–17) are relative to the same reference period, 1980–1999, used by Chapman and Walsh (2007). While the yet-to-be released Fifth Assessment Report of the IPCC includes output from the next-generation of global climate models (CMIP5), the projections presented here are based on the more thoroughly documented CMIP3 models. The CMIP3 models have been screened for outliers in Arctic performance (Overland et al., 2011) and those outliers (e.g., FGOALS, GISS)

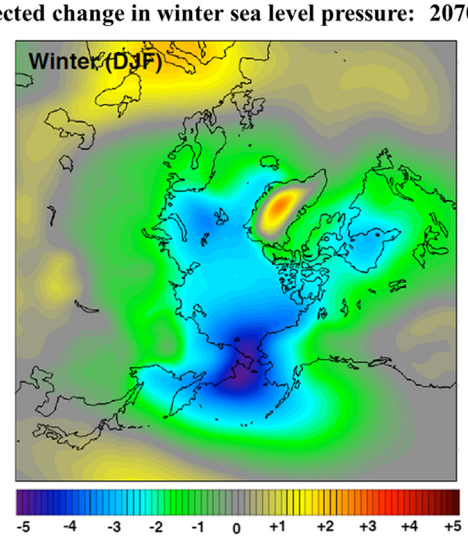

Fig. 17. Projected changes in winter sea level pressure (hPa) for 2070–2090 based on composite of CMIP3 simulations forced by the A1B scenario.

have been excluded from the model ensembles used here. Moreover, our preliminary comparisons of the Arctic projections from the CMIP3 and CMIP5 model ensembles show very similar patterns for temperature, precipitation and sea level pressure.

Fig. 15 shows the projected changes of surface air temperature by season for 2070–2090. It is apparent that warming dominates in all seasons, and the warming is polar-amplified in all seasons except in summer when the melting "ice bath" of the Arctic Ocean constrains the surface air temperature to remain close to 0 °C. Although not shown in Fig. 15, the annual mean warming is also polar-amplified, in much the same way as the observed patterns of annual warming for 1951–2010 (Fig. 4). The warming projected for 2070–2090 is largest over the Arctic Ocean in autumn and winter, consistent with a loss of summer sea ice, greater absorption of solar radiation during summer, and release of this additional heat to the atmosphere during the cold season. The winter warming pattern is highly similar to that shown for January in Bracegirdle and Stephenson's (2012) evaluation of Arctic warming in CMIP3 models under the A1B scenario, with three lobes of maximum warming: the Barents Sea, the Bering Strait region, and Hudson Bay. Fig. 15's patterns of warming in all seasons are very similar to the corresponding pattern shown in the recent Snow, Water, Ice and Permafrost in the Arctic (SWIPA) assessment report (AMAP, 2011). This Arctic Ocean warming spills over to the northern land areas, where the warming is between 2 and 3 °C during autumn and winter. This warming is 2–3 times the recent warming discussed earlier for 1951–2010, but the longer time interval to 2070–2090 makes the projected warming rate only slightly greater than the recent warming rate over Alaska/Yukon and Siberia. It should be noted that the projections in Fig. 15 are based on the A1B scenario of greenhouse gas forcing. The corresponding spatial patterns for the A2 and B1 scenarios are similar to the A1B patterns in Fig. 15, but the magnitudes of the warming are 30–50% larger (smaller) in the A2 (B1) scenario.

Fig. 16 shows the projected changes of precipitation in the 2070–2090 timeslice for summer and winter. Although precipitation fields are inherently noisier than temperature fields, the compositing of the simulations eliminates much of the spatial noise. The high latitudes are dominated by increases of precipitation in both seasons, with the largest increases found in coastal mountain ranges during winter. The only areas of precipitation decreases are in the North Atlantic south of Greenland in winter, and at the domain's periphery in summer when mid-latitude continental drying is projected by many models. The winter and summer patterns in Fig. 16 correspond closely with those shown by Kattsov et al. (2007, their Fig. 11) for the 2080–2099 time slice, although Kattsov et al.'s projections are presented as percentage changes rather than actual amounts. Accordingly, Kattsov et al. show relatively large percentage increases over during winter over the Arctic Ocean, where precipitation amounts are smaller than elsewhere in subarctic.

It should be emphasized that the projected increases of precipitation, which are typically 1–2 cm per season in the Alaska/Yukon and Siberian regions, do not preclude drying of the Arctic terrestrial regions. For example, the projected increases of precipitation over Arctic land areas shown by the IPCC (2007, Fig. 10.3) are similar to those in Fig. 16. Yet the IPCC's Fig. 10.3 shows that the same model simulations are accompanied by increases of evapotranspiration and runoff under greenhouse scenarios, resulting in decreases of soil moisture. The net hydrologic effect of a warming Arctic is an ongoing area of research, as precipitation and evapotranspiration are highly parameterized in models and hence subject to considerable uncertainties. Nevertheless, as shown in Section 3.1, there are suggestions of small increases in Arctic precipitation over the past 50–60 years, yet terrestrial drying has been sufficient to impact lake levels and fire frequencies in at least some Arctic terrestrial regions. Specifically, lake levels in the Arctic have shown a general decrease, especially in the discontinuous permafrost zone (Smith et al., 2005; Riordan et al., 2006; White et al., 2007), while the past decade has seen an increase in the frequency of severe wildfire years in Alaska (Kasischke and Turetsky, 2006; Chapin et al., 2008; USGCRP, 2009). Both changes are attributable to the increasing surface moisture deficit during summer, when evapotranspiration is comparable to, and often exceeds, precipitation over much of both terrestrial regions in this study (Serreze et al., 2003a,b).

Finally, Fig. 17 shows the projected changes of wintertime sea level pressure. The winter season is chosen here for consistency with the emphasis on the winter season advective forcing in Section 3.2. The outstanding feature of Fig. 17 is the maximum of pressure decreases ($\sim$4 hPa, averaged over all models) in the Bering Sea region. These changes are the largest in the Northern Hemisphere, and they have potentially important implications for temperatures and precipitation in the two terrestrial regions of interest in this study. Specifically, the pressure changes in Fig. 17 will

favor enhanced winter warming and precipitation in the Alaska/Yukon and Bering Strait regions, and reduced warming and precipitation west of the Bering Strait in eastern Siberia. Such a pattern of differential warming has been shown to be already underway during winter (Fig. 5a). However, the projected temperature changes in Fig. 15a contain a maximum over the Bering Strait region, which is a region of wintertime sea ice loss in most CMIP3 models. The projected pattern of warming thus indicates that sea ice loss will have a greater impact on winter temperature changes than will changes in the surface winds in high-latitude ocean areas. The pressure changes in Fig. 17 are also indicative of increased storm activity in the Bering region. Areas vulnerable to increased storminess include the western coast of Alaska and the eastern coast of Siberia. The role of changes in cyclone activity in these areas has received relatively little attention, but the receding sea ice cover along these coasts raises the possibility that, with regard to the vulnerability of coastal communities, impacts of changes in storminess could outweigh the direct impacts of warming and/or increases in seasonal mean precipitation.

4. Summary

This study was intended to synthesize information on climate changes in two Arctic terrestrial regions that are foci of climate and ecosystem research on a variety of scales, ranging from point measurements to the plot and landscape studies that can be further upscaled. While the latitudes and ecosystems of these two regions have commonalities, the regions are separated by distances greater than the scale of weather systems that are the building blocks of climate. The results presented in Section 3 provide a consistent picture of ongoing and projected changes in Alaska/Yukon and eastern Siberia. Over the timescale of 60 years (1950–2010), the trends of temperature and precipitation in the two regions are broadly similar, although atmospheric advection has been shown to influence the two regions differently during winter. The differential advective effects are much weaker in the other seasons, and they play essentially no role in the warm season. The Pacific Decadal Oscillation is the strongest correlator with interannual variability in the two regions, followed by the Arctic Oscillation and the El Niño/Southern Oscillation.

Projected changes by the late 21st Century are qualitatively similar to the changes that have been ongoing over the past 60 years, although the rate of change increases modestly under mid-range forcing scenarios (e.g., the A1B scenario). While the greatest warming is projected to occur farther north over the Arctic Ocean in response to sea ice loss, the proximity of Alaska/Yukon and eastern Siberia to the increasingly ice-free oceans leads to some amplification of the warming over these land areas. Precipitation is projected to increase by all models, although increases in evapotranspiration preclude conclusions about wetter or drier land surface conditions. A notable feature of the future climate simulations is a bulls-eye of pressure decreases in the Bering Sea region, raising the possibility of increased storminess and advectively driven changes in wintertime climate in the coastal areas of both terrestrial regions.

Acknowledgments

This work was supported by the JAMSTEC-IARC Collaborative Study and by the National Science Foundation's Division of Polar Programs through Grant ARC-1023131.

References

ACIA, 2005. The Arctic Climate Impact Assessment. Scientific Report. Arctic Monitoring and Assessment Programme, Cambridge University Press, Cambridge, U.K., p. 1042.

AMAP, 2011. Snow, Water, Ice and Permafrost in the Arctic, Scientific Report. Arctic Monitoring and Assessment Programme, Cambridge University Press, Cambridge, U.K.. Available at: http://amap.no/swipa/

Bekryaev, R.V., Polyakov, I.V., Alexeev, V.A., 2010. Role of polar amplification in long-term surface air temperature variations and modern Arctic warming. J. Clim. 23, 3888–3906.

Bracegirdle, T.J., Stephenson, B.D., 2012. Higher precision estimates of regional polar warming by ensemble regression of climate model projections. Clim. Dyn.. http://dx.doi.org/10.1007/s00382-012-1330-3.

Bromwich, D.H., Fogt, R.L., Hodges, K.I., Walsh, J.E., 2007. A tropospheric assessment of the ERA-40, NCEP and JRA-25 global reanalyses in the polar regions. J. Geophys. Res. 112. http://dx.doi.org/10.1029/2006JD007859.

Chapman, W.L., Walsh, J.E., 2007. Simulations of Arctic temperature and pressure by global coupled models. J. Clim. 20, 609–632.

Chapin III, F.S., Trainor, S.F., Huntington, O., Lovecraft, A.L., Zavaleta, E., Natcher, D.C., McGuire, A.D., Nelson, J.L., Lily, R., Calef, M., Fresco, N., Huntington, H., Rupp, T.S., DeWild, L., Naylor, R.L., 2008. Increasing wildfire in Alaska's boreal forest: pathways to potential solutions of a wicked problem. BioScience 58, 531–540.

Ebisuzaki, W., 1997. A method to estimate the statistical significance of a correlation when the data are serially correlated. J. Clim. 10, 2147–2153.

Gleicher, K.J., Walsh, J.E., Chapman, W.L., 2011. A vorticity-based analysis of the spatial and temporal characteristics of the

Beaufort anticyclone. J. Geophys. Res. 116, D18115. http://dx.doi.org/10.1029/2011JD015709.

Hartmann, B., Wendler, G., 2005. The significance of the 1976 Pacific climate shift in the climatology of Alaska. J. Clim. 18, 4824–4839.

Hinzman, L.D., Ohata, T., Polyakov, I.V., Suzuki, R., Walsh, J.E., 2013. JAMSTEC-IARC international collaboration enhancing understanding of the Arctic climate system. Polar Sci. 7 (2), 49–52.

Hirabayashi, Y., Kanae, S., Motoya, K., Masuda, K., Doll, P., 2008. A 59-year (1948–2006) global near-surface meteorological data set for land surface models, part I: development of daily forcing and assessment of precipitation intensity. Hydrol. Res. Lett. 2, 36–40.

IPCC, 2007. Climate change 2007: the physical science basis. In: Solomon, S., et al. (Eds.), Contribution of Working Group I to the Fourth Assessment Report of the Intergovernmental Panel on Climate Change. Cambridge University Press, Cambridge, U.K. and New York, p. 996.

Kalnay, E., Kanamitsu, M., Kistler, R., Collins, W., Deaven, D., Gandin, L., Iredell, M., Saha, S., White, G., Woolen, J., Zhu, Y., Chelliah, M., Ebisuzaki, W., Higgins, W., Janowiak, J., Mo, K.C., Ropelewski, C., Wang, J., Leetmaa, A., Reynolds, R., Jenne, R., Joseph, D., 1996. The NCEP/NCAR 40-year reanalysis project. Bull. Amer. Meteor. Soc. 77, 437–471.

Kasischke, E.S., Turetsky, M.R., 2006. Recent changes in the fire regime across the North American boreal region – spatial and temporal patterns of burning across Canada and Alaska. Geophys. Res. Lett. 33, L09703. http://dx.doi.org/10.1029/2006GL025677.

Kattsov, V.M., Walsh, J.E., Chapman, W.L., Govorkova, V.A., Pavlova, T.V., Zhang, X., 2007. Simulation and projection of Arctic freshwater budget components by the IPCC AR4 global climate models. J. Hydrometeor. 8, 5710589.

Kistler, R., Kalnay, E., Collins, W., Saha, S., White, G., Woollen, J., Chelliah, M., Ebisuzaki, W., Kanamitsu, M., Kousky, V., van den Dool, H., Jenne, R., Fiorino, M., 2001. The NCEP-NCAR 50-year reanalysis: monthly means CD-ROM and documentation. Bull. Amer. Meteor. Soc. 82, 247–267.

Lu, C.-H., Kanamitsu, M., Roads, J.O., Ebisuzaki, W., Mitchell, K.M., Lohmann, D., 2005. Evaluation of soil moisture in the NCEP-NCAR and NCEP-DOE global reanalyses. J. Hydrometeor. 6, 391–408.

Maurer, E.P., O'Donnell, G.M., Lettenmaier, D.P., Roads, J.O., 2001. Evaluation of the land surface water budget in NCEP/NCAR and NCEP/DOE reanalyses using an off-line hydrologic model. J. Geophys. Res. 106, 17,841–17,862.

Mesquita, M.D.S., Atkinson, D.E., Hodges, K.I., 2010. Characteristics and variability of storm tracks in the North Pacific, Bering Sea and Alaska. J. Clim. 23, 294–311.

Overland, J.E., Wang, M., Bond, N.A., Walsh, J.E., Kattsov, V.M., Chapman, W.L., 2011. Considerations in the selection of global climate models for regional climate projections: the Arctic as a case study. J. Clim. 24, 1583–1597.

Park, H., Walsh, J., Kim, Y., Nakai, T., Ohata, T., 2013. The role of declining Arctic sea ice in recent decreasing terrestrial Arctic snow depths. Polar Sci. 7 (2), 174–187.

Riordan, B., Verbyla, D., McGuire, A.D., 2006. Shrinking ponds in subarctic Alaska based on 1950–2002 remotely sensed images. J. Geophys. Res. 111, G04002. http://dx.doi.org/10.1029/2005JG000150.

Serreze, M.C., Barrett, A., Lo, F., 2005. Northern high latitude precipitation as depicted by atmospheric reanalyses and satellite retrievals. Mon. Weather Rev. 133, 3,407–3,430.

Serreze, M.C., Bromwich, D.H., Clark, M.P., Etringer, A.J., Zhang, T., Lammers, R., 2003a. Large-scale hydro-climatology of the terrestrial Arctic drainage system. J. Geophys. Res. 108. http://dx.doi.org/10.1039/2001JD000919.

Serreze, M.C., Clark, M.P., Bromwich, D.H., 2003b. Monitoring precipitation over the Arctic terrestrial drainage system: data requirements, shortcomings, and applications of atmospheric reanalysis. J. Hydrometeor. 4, 387–407.

Shiklomanov, A.I., Lammers, R.B., Rawlins, M.A., Smith, L.C., Pavelsky, T.M., 2007. Temporal and spatial variations in maximum river discharge from a new Russian data set. J. Geophys. Res. 112, G04S53. http://dx.doi.org/10.1029/2006JG000352.

Smith, L.C., Sheng, Y., MacDonald, G.M., Hinzman, L.D., 2005. Disappearing arctic lakes. Science 308, 1429.

Stroeve, J.C., Serreze, M.C., Holland, M.M., Kay, J.E., Maslanik, J., Barrett, A.P., 2011. The Arctic's rapidly shrinking ice cover: a research synthesis. Clim. Change. http://dx.doi.org/10.1007/s10584-011-0101-1.

Thompson, D.W.J., Wallace, J.M., 2000. Annular modes in the extratropical circulation. Part I: month-to-month variability. J. Clim. 13, 1000–1016.

USGCRP, 2009. Global Climate Change Impacts in the United States. U. S. Global Change Research Program, Cambridge University Press, p. 188.

Walsh, J.E., Overland, J.E., Groisman, P.V., Rudolf, B., 2011. Ongoing climate change in the Arctic. Ambio 40, 6–16.

White, D., Hinzman, L., Alessa, L., Cassano, J., Chambers, M., Falkner, K., Francis, J., Gutowski Jr., W.J., Holland, M., Holmes, R.M., Huntington, H., Kane, D., Kliskey, A., Lee, C., McClelland, J., Peterson, B., Rupp, T.S., Straneo, F., Steele, M., Woodgate, R., Yang, D., Yoshikawa, K., Zhang, T., 2007. The arctic freshwater system: changes and impacts. J. Geophys. Res. 112, G04S54. http://dx.doi.org/10.1029/2006JG000353.

Zhang, X., He, J., Zhang, J., Polyakov, I., Gerdes, R., Inoue, J., Wu, P., 2013. Enhanced poleward moisture transport and amplified northern high-latitude wetting trend. Nat. Clim. Change 3, 47–51.

Zhang, X., Walsh, J.E., Zhang, J., Bhatt, U.S., Ikeda, M., 2004. Climatology and interannual variability of Arctic cyclone activity. J. Clim. 17, 2300–2317.